Double-Q 120 degrees structure in the Heisenberg antiferromagnet on rhombohedrally stacked triangular lattice $LiCrO_2$

1995 J. Phys.: Condens. Matter 7 6869

(http://iopscience.iop.org/0953-8984/7/34/011)

J. Phys.: Condens. Matter 7 (1995) 6869–6884. Printed in the UK

Double-Q 120° structure in the Heisenberg antiferromagnet on rhombohedrally stacked triangular lattice $LiCrO_2$

Hiroaki Kadowaki†, Humihiko Takei† and Kiyoichiro Motoya‡§

† Institute for Solid State Physics, The University of Tokyo, Roppongi, Minato-ku, Tokyo 106, Japan

‡ Department of Physics, Faculty of Science, Saitama University, 255 Shimo-Okubo, Urawa, Saitama 338, Japan

Received 22 September 1994, in final form 1 June 1995

Abstract. The magnetic ordering of the $S = \frac{3}{2}$ Heisenberg antiferromagnet on a rhombohedrally stacked triangular lattice $LiCrO_2$ is studied by susceptibility, neutron diffraction and polarization analysis measurements using a single crystal. The temperature dependence of the susceptibility strongly suggests that a 120° structure is established in each quasi-two-dimensional layer, which is parallel to the c plane. Assuming the 120° structure in which magnetic moments are confined in a plane including the c axis because of an Ising-type anisotropy, neutron scattering shows that the magnetic ordering is a double-Q structure with non-equivalent wave numbers $q = (\frac{1}{3}\frac{1}{3}0)$ and $(-\frac{2}{3}\frac{1}{3}\frac{1}{2})$. It is characterized by an alternating sequence of rotational direction of the 120° structure along the c axis.

1. Introduction

Antiferromagnets on a purely two-dimensional (2D) triangular lattice have been shown to have interesting magnetic properties [1–4]. For classical ($S = \infty$) XY or Heisenberg spins, the ground-state magnetic ordering is the non-collinear 120° structure, in which three sublattice spins rotate 120° from one another. Because of this 120° structure, phase transitions in the 2D triangular lattice show interesting behaviour [2, 3]. If this triangular lattice is stacked rhombohedrally, ABCABC stacking, and a weak interlayer exchange coupling is introduced, the three-dimensional magnetic structure becomes a complicated problem. If the 120° structure is preserved in the layer, each molecular field from first- and second-neighbouring layers is cancelled out. Consequently the magnetic ordering is governed by subtle balances and small perturbations.

The problem of the quasi-2D rhombohedral antiferromagnet was studied by Rastelli and Tassi [5] for nearest-neighbour intralayer (J) and interlayer (J') exchange couplings (see only Cr sites of figure 1). They showed that the classical ground state is the single-Q helical ordering

$$S_R = a\,e^{iq\cdot R} + a^*\,e^{-iq\cdot R} \tag{1}$$

where a is a complex polarization vector $a = a' - ia''$ with real vectors a' and a'' which are $|a'| = |a''|$ and $a' \perp a''$. The wave number q has infinite degeneracy on a degeneration

§ Present address: Department of Physics, Faculty of Science and Technology, Science University of Tokyo, Noda 278, Japan.

0953-8984/95/346869+16$19.50

line

$$q = \left(\frac{1}{3}, \frac{1}{3}, \zeta\right) + \left(u/3 - v/\sqrt{3}, u/3 + v/\sqrt{3}, 0\right)$$
$$u = \frac{\sqrt{3}J'}{2\pi J}\cos\left(\frac{2\pi\zeta}{3}\right) \qquad v = -\frac{\sqrt{3}J'}{2\pi J}\sin\left(\frac{2\pi\zeta}{3}\right) \tag{2}$$

for small J'. A slightly incommensurate modulation ($u, v \neq 0$) in the c plane produces an interlayer molecular field and stabilizes the classical energy. The infinite degeneracy is lifted by perturbations such as the quantum correction [5], a magnetic field perpendicular to the c axis [5] and further-neighbour exchange interactions [6]. They stabilize a point on the degeneration line (2) at either $\zeta = 0$ or $\zeta = \frac{1}{2}$

The Heisenberg antiferromagnet on the quasi-2D rhombohedral lattice is realized in some Cr compounds, $ACrO_2$ (A = Li, Na, K) [7–11] of the α-$NaFeO_2$ structure, illustrated in figure 1, and $MCrO_2$ (M = Cu, Ag) [12–14] of the delafossite structure. Magnetic structures of $CuCrO_2$ [13] and $AgCrO_2$ [14] were studied by powder neutron diffraction. Magnetic reflections of $CuCrO_2$ are well described by the $Q = (\frac{1}{3}\frac{1}{3}l = 0, 1, 2, \ldots)$ series, which are consistent with the above scenario for small J'/J. The magnetic modulation of $AgCrO_2$ is $Q = (0.327, 0.327, 0)$, which suggests a slight modulation of the three-sublattice structure due to a larger interlayer coupling.

On the other hand, neutron diffraction on powder [8] and single-crystalline [9] samples of $LiCrO_2$ showed that there are non-equivalent two modulations $Q = (\frac{1}{3}\frac{1}{3}l)$, $l = 0$ and $l = \frac{1}{2}$. This implies either that magnetic ordering of $LiCrO_2$ consists of two domains with $l = 0$ and $\frac{1}{2}$, or that a multi-Q structure is established. The single-crystal neutron diffraction [9] showed that there is 2D diffuse scattering as a scattering rod along $Q = (\frac{1}{3}\frac{1}{3}\zeta)$ around T_N, and proved the 2D character, which was expected from the crystal structure illustrated in figure 1. Because of this 2D character and the Heisenberg nature of Cr^{3+} spins, it is expected that magnetic ordering in each triangular plane, parallel to the c plane, is the 120° structure in which magnetic moments are confined either in the c plane or in a plane including the c axis, which depends on the anisotropy. However the proposed magnetic structure from the single-crystal study [9] is quite different from this expectation. It is a superposition of the 120° structure in the c plane and a magnetic ordering of the c axis component. To resolve this discrepancy, we re-examined the magnetic ordering of $LiCrO_2$ using a newly prepared single crystal by means of neutron diffraction and magnetic susceptibility measurement, which has not been reported for a single crystal. In addition to the standard neutron diffraction technique, we utilized polarization analysis, by which one can unambiguously distinguish between the 120° structures in the c plane and in a plane including the c axis.

2. Experimental details

Single crystals of $LiCrO_2$ were grown by the Li_2O–PbO–B_2O_3 flux method. A typical starting composition of the solution was 0.065 mol of Li_2CO_3, 0.014 mol of PbO, 0.034 mol of B_2O_3 and 0.22 mol of Cr_2O_3. The reagents were mixed and packed into a 50 ml Pt crucible and heated in an electric furnace to 1300 °C for 24 hours in air. After soaking, the furnace was cooled at a rate of 3 °C h^{-1} to 800 °C, and then naturally cooled to room temperature. The crystals were separated from the solidified flux by leaching the crucible in hot and dilute HNO_3 for several hours. The obtained crystals were checked with single-crystal x-ray diffraction and scanning electron microscope analyses. The specimen used in

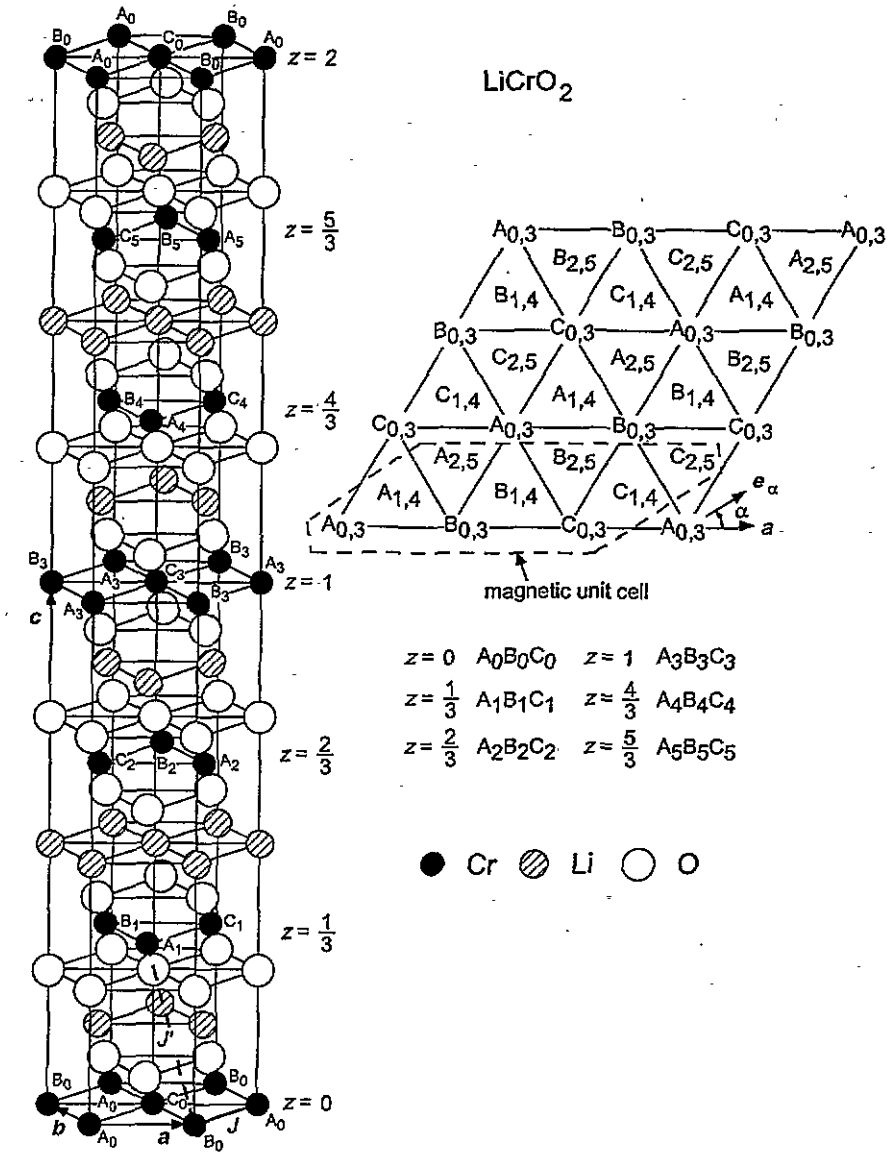

Figure 1. Crystal structure of $LiCrO_2$ and 18 sublattices of magnetic structure. Cr sites form a rhombohedral lattice. The 18 sublattices are represented by A_n, B_n and $C_n (n = 0, 1, \ldots, 5)$, and are also shown by projection along the c axis. Thick solid and dashed lines represent *nearest-neighbour exchange interactions in the c plane, J, and between the c planes, J'. e_α is a* direction in the c plane rotated by an angle α from the a axis, and is used to show model spin structures drawn in figure 5.

this experiment was 11 mm^3 in volume.

Magnetic susceptibility was measured in a magnetic field of 2 T using a commercial Quantum Design Co. SQUID magnetometer. Unpolarized neutron diffraction experiments were performed on the ISSP-GPTAS triple-axis spectrometer installed at JRR-3M JAERI (Tokai) with the double-axis configuration. A pyrolytic graphite (0 0 2) reflection was used

for the monochromator. Higher-order neutrons were removed by the pyrolytic graphite filter. The neutron energy was fixed at either 13.7 or 30.5 meV, and collimations 30′–40′–40′ were employed. A polarization analysis experiment was carried out on the ISSP- PONTA spectrometer at JRR-3M using a Heusler polarizer. Neutrons of 13.7 meV and collimations 30′–80′–80′–80′ were used. Higher-order neutrons were removed by the pyrolytic graphite filter. The sample was mounted in a closed cycle ^{4}He gas refrigerator, so that the horizontal scattering plane of the spectrometer coincided with the $(h\,h\,l)$, $(h\,0\,l)$ or $(h\,k\,0)$ zone.

3. Experimental results

3.1. Magnetic susceptibility

The temperature dependence of the magnetic susceptibility is shown in figure 2. The susceptibility is almost temperature independent, and shows no anisotropy above T_N and a very small anisotropy $\chi_{\parallel c} > \chi_{\perp c}$ below T_N. No anisotropy and very weak temperature dependence of the susceptibility are well known characteristics of the Heisenberg antiferromagnet on the 2D triangular lattice. These were shown by a Monte Carlo simulation [3] and were observed in the real antiferromagnets VBr_2 and VCl_2 [15]. Therefore the susceptibility data strongly suggest that $LiCrO_2$ is a good quasi-2D system.

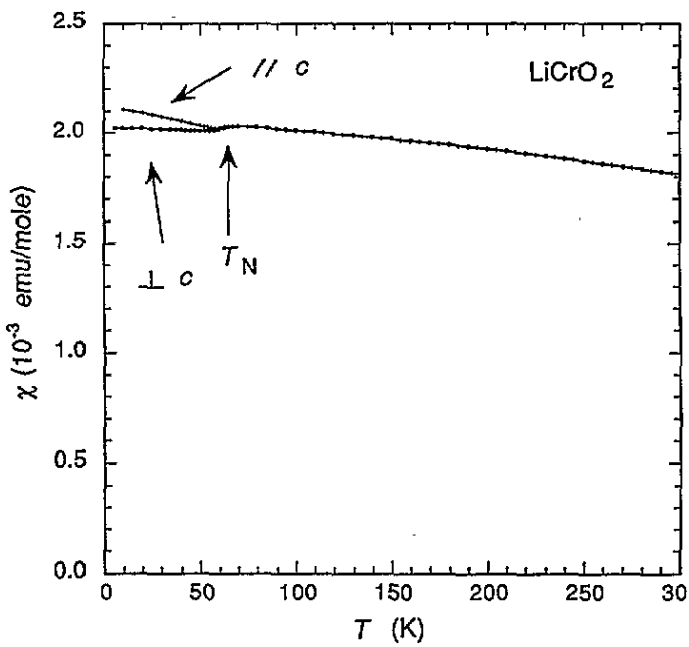

Figure 2. Temperature dependence of magnetic susceptibility.

3.2. Unpolarized neutron diffraction

Crystal structure refinement of $LiCrO_2$ was performed by both the previous neutron powder [8] and single-crystal [9] experiments. To confirm their results, we also performed it using $(h\,0\,l)$-type reflections, and obtained the same result. It is summarized in table 1.

Table 1. Observed and calculated squares of structure factors of $LiCrO_2$ at $T = 300$ K (space group, $R\bar{3}m$; atomic positions, Cr (0, 0, 0), Li (0, 0, $\frac{1}{2}$) and O (0, 0, z) $z = 0.2575(3)$).

hkl	$\lvert F\rvert^2_{obs}$	$\lvert F\rvert^2_{calc}$
003	6.2	4.6
006	8.0	8.0
009	0.059	0.050
107	7.1	7.8
104	12	16
101	3.1	2.2
$10\bar{2}$	10.6	8.7
$10\bar{5}$	0.83	0.71
$10\bar{8}$	11	14
205	0.61	0.71
202	8.8	8.7
$20\bar{1}$	2.9	2.2
$20\bar{7}$	8.2	7.8

Magnetic reflections of $LiCrO_2$ were observed at $(\frac{1}{3}\frac{1}{3}l)$ and $(\frac{2}{3}\frac{2}{3}l)$ with $l = 0, \pm\frac{1}{2}, \pm1, \pm\frac{3}{2}, \pm2, \ldots$ as reported in the previous work [9]. By scans along $(\frac{1}{3}, \frac{1}{3}, \zeta)$, (ξ, ξ, l) and $(\frac{1}{3}+\xi, \frac{1}{3}-\xi, 0)$, we recognized that the magnetic Bragg scattering is not resolution limited along the c axis. Typical scans through $(\frac{1}{3}\frac{1}{3}0)$ are shown in figure 3. The scan along the [110] direction is resolution limited, whereas the scan along the c axis clearly shows broadening. The profiles were fitted by a Gaussian form $\delta(\Delta Q_{\perp c})\exp[-(\Delta Q_{\parallel c}/\kappa_{\parallel c})^2]$ convoluted with the instrumental resolution which was measured using the nuclear Bragg scattering. The convoluted profiles are also plotted in figure 3. The fitted parameter is $\kappa_{\parallel c} = 0.023$ r.l.u. $= 0.0098$ Å^{-1}. We notice that profiles of other reflections with $l = \frac{1}{2}, 1, \frac{3}{2}, 2, \ldots$ can be fitted by this value. The correlation length of the magnetic ordering along the c axis is about $1/\kappa_{\parallel c} = 100$ Å. We think that the finite correlation length is brought about by certain randomness such as impurities and defects of the lattice, which easily destroys weak interlayer coupling.

As discussed in the introduction, a displacement of the magnetic reflection from the commensurate $(\frac{1}{3}\frac{1}{3}0)$ on the c plane may be observed. We checked this possibility in the $(hk0)$ zone, but did not detect any displacement. Experimental upper limits of the displacement are $|\Delta Q_l| < 0.007$ Å^{-1} and $|\Delta Q_t| < 0.005$ Å^{-1} along the [110] and [1$\bar{1}$0] directions, respectively. If we apply equation (2), the ratio of the exchange constants is $|J'/J| < 0.018$.

The temperature dependence of peak intensities of the magnetic reflections at $(\frac{1}{3}\frac{1}{3}l)$, $l = 0, \frac{1}{2}, 3, \frac{7}{2}$, is shown in figure 4. The peak intensities were measured by scans along $(\frac{1}{3}\frac{1}{3}\zeta)$. Diffuse-scattering parts were subtracted from the data. As temperature is decreased, they all appear from the Néel temperature $T_N = 64$ K and relative intensities are constant within the experimental error. This can be interpreted as indicating that the magnetic ordering is not a multidomain type with non-equivalent $l = 0$ and $\frac{1}{2}$ modulations but a multi-Q structure including both the modulations. The feature that the intensity does not saturate, even below $T_N/2$, reflects the finite correlation length of the magnetic Bragg scattering.

Neutron scattering intensities of magnetic reflections were measured by θ–2θ scans and scans along the c direction at $T = 10$ K. The absolute intensity was obtained by fitting the scattering profiles to the Gaussian form convoluted with the instrumental resolution as

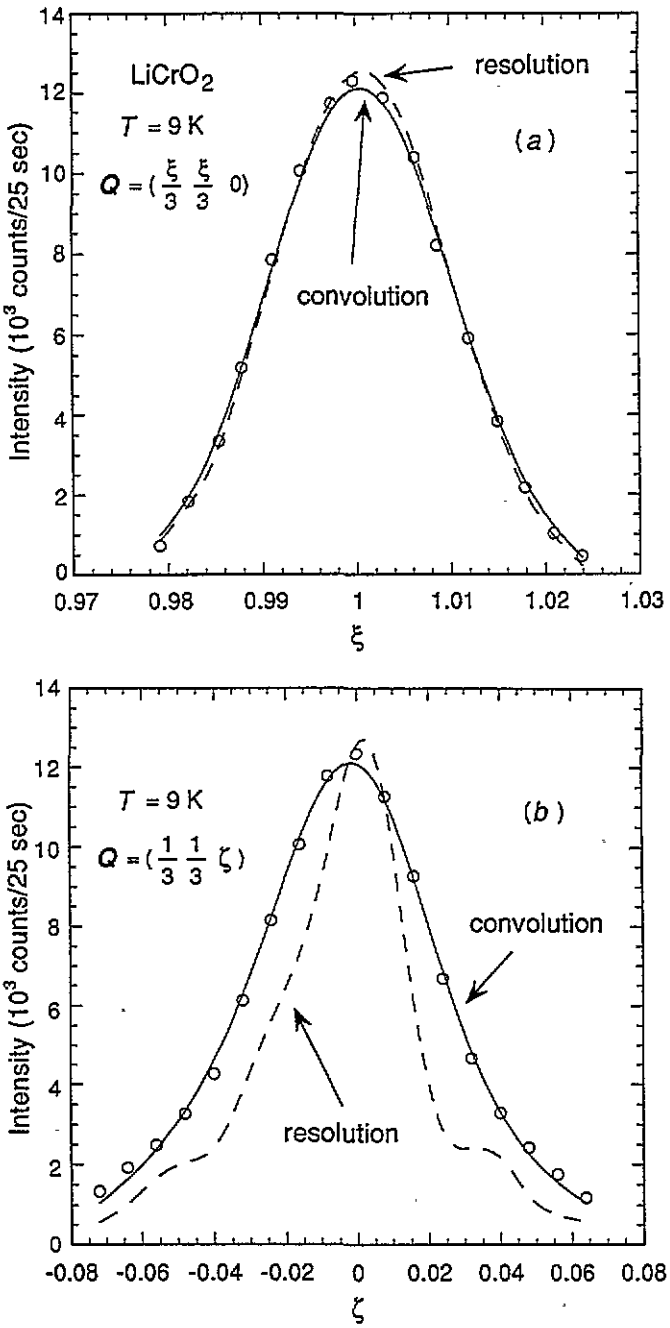

Figure 3. Scans through the $(\frac{1}{3}\frac{1}{3}0)$ magnetic reflection along (*a*) [110] and (*b*) [001] directions. Dashed and solid lines are fits to the resolution and the Gaussian function $\delta(\Delta Q_{\perp c})\exp[-(\Delta Q_{\parallel c}/\kappa_{\parallel c})^2]$ convoluted with the resolution, respectively.

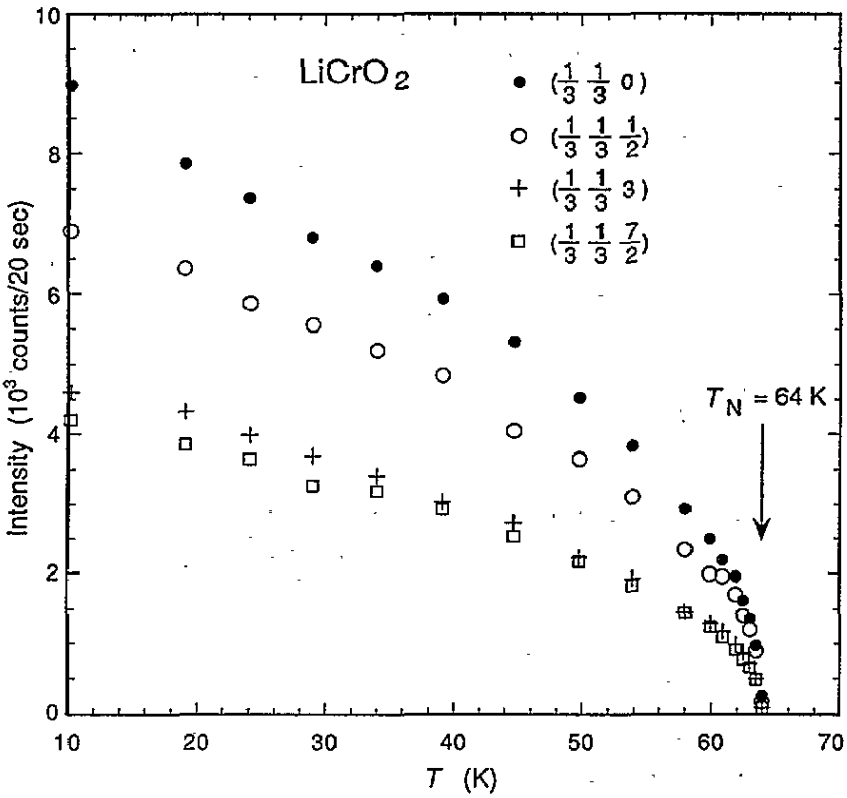

Figure 4. Temperature dependence of intensity of magnetic reflections at $(\frac{1}{3}\frac{1}{3}l)$, $l = 0, \frac{1}{2}, 3$ and $\frac{7}{2}$.

shown in figure 3. It was corrected for the absorption. The intensity is written as

$$I \propto \left(\frac{g}{2} f(Q)\right)^2 [|F_{M\perp}(Q)|^2]_{av}$$

$$F_M(Q) = \sum_{\text{magnetic unit cell}} S_R \, e^{iQ\cdot R} \qquad F_{M\perp}(Q) = F_M(Q) - \hat{Q}(\hat{Q}\cdot F_M(Q)) \tag{3}$$

where g and $f(Q)$ are the g factor and form factor of Cr^{3+} respectively, and $[]_{av}$ stands for an average over multidomains. The intensity was divided by the square of the form factor $f(Q)$ approximated by calculation [16], and is listed as $|F_M|^2_{obs} = (g/2)^2[|F_{M\perp}(Q)|^2]_{av}$ in table 2.

3.3. Polarized neutron diffraction

In order to directly measure components of $F_{M\perp}(Q)$, we carried out the polarization analysis. Spin flip and non-flip scattering of magnetic reflections were measured at $T = 10$ K. They are given by

$$I_{\uparrow\uparrow} = I_{\downarrow\downarrow} \propto [|e\cdot F_{M\perp}(Q)|^2]_{av} \qquad I_{\uparrow\downarrow} = I_{\downarrow\uparrow} \propto [|F_{M\perp}(Q)|^2 - |e\cdot F_{M\perp}(Q)|^2]_{av} \tag{4}$$

where $I_{\uparrow\downarrow}$, for example, stands for the intensity of down-spin neutrons scattered from the up-spin state, and e is a unit vector along the neutron spin, which is parallel to the guide field. Terms coming from $e\cdot[F^*_{M\perp}(Q)\times F_{M\perp}(Q)]$ are neglected, because they vanish after

Table 2. *Observed and calculated squares of magnetic structure factors of* $LiCrO_2$ *at* $T = 10$ K. Calculated values are for the model structures shown in figure 5(*a*), (*b*) and (*e*).

		$\lvert F_M\rvert^2_{calc}$		
hkl	$\lvert F_M\rvert^2_{obs}$	(*a*)	(*b*)	(*e*)
$\frac{1}{3}\frac{1}{3}0$	0.41(0.04)	0.22	0.39	0.39
$\frac{1}{3}\frac{1}{3}\frac{1}{2}$	0.34(0.03)	0.08	0.33	0.33
$\frac{1}{3}\frac{1}{3}1$	0.32(0.03)	0.14	0.31	0.30
$\frac{1}{3}\frac{1}{3}\frac{3}{2}$	0.37(0.04)	0.12	0.35	0.35
$\frac{1}{3}\frac{1}{3}2$	0.075(0.007)	0.133	0.079	0.076
$\frac{1}{3}\frac{1}{3}\frac{5}{2}$	0.086(0.009)	0.076	0.077	0.078
$\frac{1}{3}\frac{1}{3}3$	0.34(0.03)	0.17	0.32	0.32
$\frac{1}{3}\frac{1}{3}\frac{7}{2}$	0.36(0.04)	0.07	0.37	0.37
$\frac{1}{3}\frac{1}{3}4$	0.40(0.04)	0.12	0.39	0.39
$\frac{1}{3}\frac{1}{3}\frac{9}{2}$	0.23(0.02)	0.09	0.23	0.23
$\frac{1}{3}\frac{1}{3}5$	0.083(0.008)	0.121	0.086	0.086
$\frac{1}{3}\frac{1}{3}\frac{11}{2}$	0.038(0.004)	0.070	0.035	0.039
$\frac{1}{3}\frac{1}{3}6$	0.27(0.03)	0.14	0.28	0.28
$\frac{1}{3}\frac{1}{3}\frac{13}{2}$	0.25(0.03)	0.07	0.30	0.31
$\frac{2}{3}\frac{2}{3}0$	0.40(0.04)	0.22	0.39	0.39
$\frac{2}{3}\frac{2}{3}\frac{1}{2}$	0.27(0.03)	0.08	0.26	0.26
$\frac{2}{3}\frac{2}{3}1$	0.16(0.02)	0.14	0.17	0.16
$\frac{2}{3}\frac{2}{3}\frac{3}{2}$	0.38(0.04)	0.13	0.38	0.38
$\frac{2}{3}\frac{2}{3}2$	0.30(0.03)	0.14	0.31	0.30
$\frac{2}{3}\frac{2}{3}3$	0.36(0.04)	0.20	0.36	0.36

taking the average on domains corresponding to the inversion symmetry. The polarization analysis measurement was carried out in the (*hhl*) zone with a vertical guide field along the $[1\bar{1}0]$ direction. The results were corrected for the instrumental depolarization, and are listed as $I_{\uparrow\uparrow}/(I_{\uparrow\uparrow} + I_{\uparrow\downarrow})$ in table 3.

A few data of the polarization analysis provide an important qualitative conclusion. If the wave number Q is nearly perpendicular to the c axis, such as $Q = (\frac{1}{3}\frac{1}{3}l)$ and $(\frac{2}{3}\frac{2}{3}l)$ with $l = 0$ and $\frac{1}{2}$, $I_{\uparrow\uparrow}$ and $I_{\uparrow\downarrow}$ detect ordering in the c plane and along the c axis, respectively. From table 3, one sees that both $I_{\uparrow\uparrow}$ and $I_{\uparrow\downarrow}$ for small l are finite. Therefore we conclude that the magnetic structure has components both along the c axis and in the c plane.

4. Analysis of magnetic structure

4.1. Requirement of magnetic structure

The indexes of magnetic reflections, $(\frac{1}{3}\frac{1}{3}l)$, $l = 0, \pm\frac{1}{2}, \pm1, \pm\frac{3}{2}, \pm2, \ldots$, imply that the magnetic unit cell contains 18 sublattice Cr sites, three sublattices in a layer and six layers, which are illustrated in figure 1 by A_n, B_n and C_n ($n = 0, 1, 2, 3, 4, 5$). Coordinates of the 18 sublattice sites, R_{A_n}, R_{B_n} and R_{C_n} at A_n, B_n and C_n ($n = 0, 1, 2, 3, 4, 5$) respectively, are $R_{A_0} = (000)$, $R_{A_1} = (\frac{2}{3}\frac{1}{3}\frac{1}{3})$, $R_{A_2} = (\frac{4}{3}\frac{2}{3}\frac{2}{3})$, $R_{A_3} = (001)$, $R_{A_4} = (\frac{2}{3}\frac{1}{3}\frac{4}{3})$, $R_{A_5} = (\frac{4}{3}\frac{2}{3}\frac{5}{3})$, $R_{B_n} = R_{A_n} + (100)$ and $R_{C_n} = R_{A_n} + (200)$.

No magnetic reflection is observed at $Q = (00l)$ and $(11l)$, $l = 0, \pm\frac{1}{2}, \pm1, \pm\frac{3}{2}, \pm2, \ldots$.

Table 3. Observed and calculated values of $I_{\uparrow\uparrow}/(I_{\uparrow\uparrow}+I_{\uparrow\downarrow})$ of $LiCrO_2$ at $T = 10$ K. Calculated values are for the model structures shown in figure 5(*a*), (*b*) and (*e*).

		$[I_{\uparrow\uparrow}/(I_{\uparrow\uparrow}+I_{\uparrow\downarrow})]_{calc}$		
hkl	$[I_{\uparrow\uparrow}/(I_{\uparrow\uparrow}+I_{\uparrow\downarrow})]_{obs}$	(*a*)	(*b*)	(*e*)
$\frac{1}{3}\frac{1}{3}0$	0.60(0.01)	0.50	0.61	0.63
$\frac{1}{3}\frac{1}{3}\frac{1}{2}$	0.09(0.01)	0.20	0.11	0.12
$\frac{1}{3}\frac{1}{3}1$	0.22(0.01)	0.21	0.21	0.21
$\frac{1}{3}\frac{1}{3}\frac{3}{2}$	0.42(0.01)	0.55	0.40	0.41
$\frac{1}{3}\frac{1}{3}2$	0.84(0.02)	0.22	0.83	0.85
$\frac{1}{3}\frac{1}{3}\frac{5}{2}$	0.44(0.02)	0.22	0.45	0.48
$\frac{1}{3}\frac{1}{3}3$	0.74(0.01)	0.64	0.74	0.75
$\frac{1}{3}\frac{1}{3}\frac{7}{2}$	0.09(0.01)	0.22	0.09	0.10
$\frac{1}{3}\frac{1}{3}4$	0.15(0.03)	0.23	0.17	0.16
$\frac{1}{3}\frac{1}{3}\frac{9}{2}$	0.57(0.05)	0.74	0.61	0.62
$\frac{2}{3}\frac{2}{3}0$	0.61(0.02)	0.50	0.61	0.63
$\frac{2}{3}\frac{2}{3}\frac{1}{2}$	0.11(0.03)	0.20	0.13	0.15
$\frac{2}{3}\frac{2}{3}1$	0.37(0.05)	0.21	0.39	0.40
$\frac{2}{3}\frac{2}{3}\frac{3}{2}$	0.38(0.03)	0.51	0.37	0.38
$\frac{2}{3}\frac{2}{3}2$	0.24(0.04)	0.21	0.21	0.21

From this extinction rule, one can easily prove that the summation of the three sublattice spins at A_n, B_n and C_n in each layer is zero,

$$S_{A_n} + S_{B_n} + S_{C_n} = 0 \tag{5}$$

where S_{A_n}, for example, stands for the sublattice spin at A_n. If this condition is satisfied, the magnetic structure can alternatively be written by a 6-Q structure

$$S_R = \sum_{j=1}^{6}(a_j\, e^{iq_j\cdot R} + a_j^*\, e^{-iq_j\cdot R}) = \sum_{j=1}^{6} 2[a_j' \cos(q_j\cdot R) + a_j'' \sin(q_j\cdot R)] \tag{6}$$

$$q_1 = \left(\frac{1}{3}, \frac{1}{3}, 0\right) \qquad q_2 = \left(-\frac{2}{3}, \frac{1}{3}, 0\right) \qquad q_3 = \left(\frac{1}{3}, -\frac{2}{3}, 0\right)$$

$$q_4 = \left(\frac{1}{3}, \frac{1}{3}, \frac{1}{2}\right) \qquad q_5 = \left(-\frac{2}{3}, \frac{1}{3}, \frac{1}{2}\right) \qquad q_6 = \left(\frac{1}{3}, -\frac{2}{3}, \frac{1}{2}\right)$$

with complex polarization vectors $a_j = a_j' - ia_j''$. Thus adjustable parameters for the magnetic structure are 12 sublattice spin vectors S_{A_n} and S_{B_n}, or equivalently 12 real vectors a_j' and a_j''.

As discussed in section 3.3, the polarization analysis shows that the ordered spins have both c axis and c plane components. As a result, the 120° structure in the c plane and ordering only along the c axis are rejected as the magnetic structure. In the following, several structure models consistent with this and the restriction (5) are fitted to data of $|F_M|^2_{obs}$ and $I_{\uparrow\uparrow}/(I_{\uparrow\uparrow}+I_{\uparrow\downarrow})$ given in tables 2 and 3. It should be noted that we calculated the average $[]_{av}$ of equations (3) and (4) by assuming that all multidomains can be derived by operating space group transformations to a model structure.

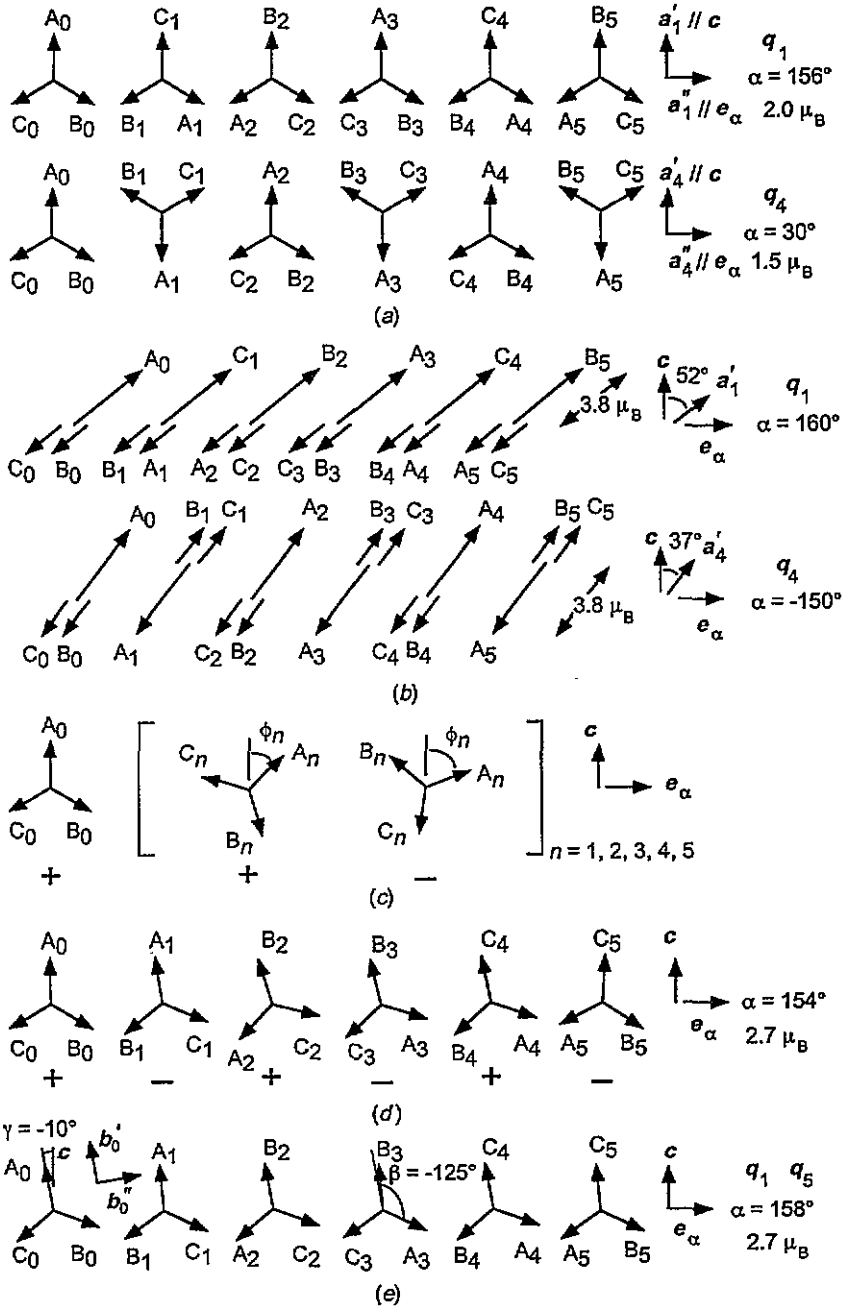

Figure 5. Magnetic structure models. 18 arrows labelled by A_n, B_n and C_n ($n = 0, 1, \ldots, 5$) represent 18 sublattice spins S_{A_n}, S_{B_n} and S_{C_n} respectively. Spins of model structures are contained in a plane including the c axis and a direction e_α in the c plane shown in figure 1. Structure parameters are values of the best-fit result. (*a*) Single-Q 120° structure with $q = q_1$ and q_4. (*b*) Single-Q structure with linear polarization for $q = q_1$ and q_4. (*c*) General 120° structure. Rotational direction is denoted by + or −. (*d*) The best-fit structure of the +−+−+− 120° structure. (*e*) Double-Q 120° structure.

4.2. Single-Q 120° structure

We consider the simplest 120° structure model described by the single-Q structure with wave numbers q_j with $j = 1, 2, \ldots, 6$. They are written by

$$S_R = a_j e^{iq_j \cdot R} + a_j^* e^{-iq_j \cdot R} = 2[a_j' \cos(q_j \cdot R) + a_j'' \sin(q_j \cdot R)]$$
$$|a_j'| = |a_j''| \qquad a_j' \perp a_j''. \tag{7}$$

From the requirement of the polarization analysis, the 120° structure should be in a plane including the c axis. Since a transformation $a_j \rightarrow e^{ix} a_j$ with any real number x does not change the intensities (3) and (4), we can impose a condition that a_j' is parallel to the c axis without loss of generality.

Least-squares fitting was performed with four parameters, spin lengths $|a_1'|$, $|a_4'|$ and directions of a_1'' and a_4'', which determine the plane containing spins. One of the least-squares solutions is shown by the 18 sublattice structures in figure 5(a). They are the single-Q 120° structures with q_1 and q_4. The other domains are derived by the threefold symmetry around the c axis. Calculated values of structure factors and $I_{\uparrow\uparrow}/(I_{\uparrow\uparrow} + I_{\uparrow\downarrow})$ for the least-squares solutions are listed in tables 2 and 3. From these values, we conclude that the observation cannot be fitted by this model. In agreement with this, the minimum value of $\chi^2 = 3034$, defined by $\chi^2 = \Sigma[(\text{obs.} - \text{calc.})/\text{error}]^2$, is far larger than $\chi^2 \approx 35$ which is required for good fitting by the χ^2 test.

4.3. Single-Q structure with linear polarization

Secondly, we consider the single-Q structure with a linear polarization, equation (7) with $a_j' \parallel a_j''$. Because of the invariance of the intensities by the transformation $a_j \rightarrow e^{ix} a_j$, we can choose $a_j'' = 0$ without loss of generality. Least-squares fitting was performed with six parameters, a_1' and a_4'. The solution is illustrated as the 18 sublattice structures in figure 5(b) for q_1 and q_4. Calculated values of structure factors and $I_{\uparrow\uparrow}/(I_{\uparrow\uparrow} + I_{\uparrow\downarrow})$ are listed in tables 2 and 3. The minimum value of $\chi^2 = 21.8$ is sufficiently small and the calculated values well reproduce the observation. However, we cannot accept this model structure, because the maximum magnetic moment, $3.8\mu_B$, is too large for Cr^{3+} which has $3\mu_B$. It should be noted that fitting with non-collinear a_j' and a_j'' was also performed, but the result did not essentially improve the collinear case.

4.4. General 120° structure

Thirdly, we consider general 120° structures in a plane including the c axis. This is illustrated in figure 5(c). The 120° structure in one layer has a discrete degree of freedom, which is the rotational direction, clockwise (+) and anti-clockwise (−). The structures are classified by a sequence of the rotational directions of the six layers. There are eight independent classes: ++++++, +++++−, ++++−−, +++−+−, ++−++−, +++−−−, ++−+−−, +−+−+−.

Least-squares fitting was performed for the eight classes, each of which has seven fitting parameters of the spin length and angles α and $\phi_n (n = 1, 2, \ldots, 5)$. The minimum of χ^2 is listed in table 4. From these values, we conclude that only the +−+−+− structure is acceptable and reproduces the observation. One of the best-fit spin configurations is shown in figure 5(d). The value of magnetic moment is $2.7\mu_B$, which is quite reasonable for the quasi-2D system. Thus we think that this model structure is the correct 120° structure sought for $LiCrO_2$.

Table 4. Minimum value of χ^2 for the general 120° structure in a plane including the c axis shown in figure 5(c).

Rotation	$++++++$	$+++++-$	$++++--$	$+++-+-$
χ^2	3036	1386	1606	580
Rotation	$++-++-$	$+++---$	$++-+--$	$+-+-+-$
χ^2	2162	1311	867	30.6

To obtain the explicit mathematical form (6) of the fitted $+-+-+-$ structures, six amplitudes $|a_j|$ were calculated for the least-squares solutions. All the solutions show that only two amplitudes for (q_1, q_5), (q_2, q_6) or (q_3, q_4) are equal and appreciable, and that the others are an order smaller. This strongly suggests that the solutions of the $+-+-+-$ structure can be well expressed by double-Q structures.

4.5. Double-Q 120° structure

Finally, we check the possibility of the double-Q 120° structure. As will be shown in the appendix, the $+-+-+-$ 120° structures with certain restrictions can be expressed by double-Q forms with wave numbers (q_1, q_5), (q_2, q_6) or (q_3, q_4). This structure for (q_1, q_5) is shown in figure 5(e). The double-Q form requires that spins at A_0, B_2 and C_4 are parallel, and that spins at A_1, B_3 and C_5 are parallel. If the double-Q 120° structure is assumed to be in a plane including the c axis, there are four structure parameters, the spin length, the angle β between S_{A_0} and S_{A_3}, the angle γ between S_{A_0} and the c axis and the angle α. As shown in the appendix, β and γ cannot be determined independently; only $\beta - 2\gamma$ can be fitted.

Least-squares fitting was performed with the three parameters, and two solutions were obtained. Calculated structure factors and $I_{\uparrow\uparrow}/(I_{\uparrow\uparrow}+I_{\uparrow\downarrow})$ are given in tables 2 and 3. They are in good agreement with the observed values, and $\chi^2 = 34$ is acceptably small. One fitted structure is shown in figure 5(e), where $\gamma = -10°$ is assumed. Its fitted parameters are magnetic moment $2.68 \pm 0.13\mu_B$ and $\beta - 2\gamma = -105 \pm 0.5°$, $\alpha = 158 \pm 3°$. The other solution has the same magnetic moment and $\beta - 2\gamma$, but a little different $\alpha = 142 \pm 3°$. Since the two values of α are not very different, one may interpret this as indicating that the difference is not intrinsic and the true value is $\alpha = 150°$. By comparing figure 5(e) and (d), one sees that the two fitting results are essentially the same. Therefore we conclude that, if the 120° structure in a plane including the c axis is assumed, neutron scattering data show that the magnetic ordering is the double-Q 120° structure characterized by the $+-+-+-$ rotational directions.

It should be noted that the fitting result of the double-Q 120° structure is also essentially the same as that of the single-Q structure with linear polarization. This is understood by the form of the complex polarization a_1 and a_5 given by equation (A7). They are collinear ($a_j' \parallel a_j''$, $j = 1, 5$). If a transformation $a_1 \rightarrow e^{-i\beta/2}a_1$ is made to the single-Q structure (7) with q_1, the resulting structure is nothing but the structure shown in figure 5(b) for q_1. Similarly a transformation $a_5 \rightarrow -e^{i(\pi-\beta)/2}a_5$ and a 120° rotation are made to the single-Q structure (7) with q_5, one reaches the structure shown in figure 5(b) for q_4.

5. Discussion

As discussed in the introduction, Soubeyroux *et al* [9] measured magnetic structure factors using a single crystal, and proposed a complicated magnetic structure. Their data cannot be quantitatively compared with our data, because they did not explicitly define structure factors. We think, however, that both sets of data are essentially the same and do not depend on the sample, because they have the characteristic feature that $(\frac{1}{3}\frac{1}{3}2)$ and $(\frac{1}{3}\frac{1}{3}\frac{5}{2})$ are weak in the $(\frac{1}{3}\frac{1}{3}l)$ series reflections. It is because of this feature that not the single-Q 120° structure but the single-Q structure with linear polarization reproduces the structure factors. Thus the point of the present work is that we have noticed that a summation of two single-Q structures with the linear polarizations can be the $+-+-+-$ 120° structure in a plane including the c axis.

From the $(3d)^3$ electronic configuration of Cr^{3+}, the anisotropy energy is expected to be the single-ion type $D(S^z)^2$. The 120° structure in a plane including the c axis indicates negative D, the Ising-like anisotropy. 120° structures in planes including the c axis are observed in other Heisenberg antiferromagnets on stacked triangular lattices, such as VCl_2 [17], $CsNiCl_3$ [18] and $RbNiCl_3$ [19], in which the stacking is the AAA...type and the spin arrangement along the c axis is the simple antiparallel sequence. In all these antiferromagnets, successive phase transitions of ordering of the c axis and c plane components commonly occur [17–19]. The successive phase transitions can be observed as the temperature dependence of intensity ratios of $I(\frac{1}{3}\frac{1}{3}l = \text{large})$ to $I(\frac{1}{3}\frac{1}{3}l = \text{small})$. No such behaviour, however, was observed in the temperature dependence of the intensities of the magnetic reflections shown in figure 4 even at $T = T_N - 0.5$ K. This can be interpreted in two ways. (1) The anisotropy parameter D is very small and the split of T_N is much smaller than 0.5 K. (2) The main anisotropy is not the single-ion-type anisotropy. There is a certain anisotropic interaction which stabilizes the double-Q 120° structure. It brings about just one phase transition.

We would like to make a few comments on the mechanism by which the double-Q 120° structure is stabilized, which remains to be studied. The double Q, for example q_1 and q_5, are not equivalent in reciprocal space, and thus $J(q_1) \neq J(q_5)$, where $J(q) = \Sigma_j J_{ij} \exp(iq \cdot R_{ij})$. As discussed in the introduction $J(q)$ takes the minimum value on the degeneration line (2), if only the nearest-neighbour intralayer (J) and interlayer (J') exchange couplings exist. Although the degeneracy is lifted by perturbations for the real system, the appearance of the double-Q structure means that the degeneracy is very weakly broken and the difference between $J(q_1)$ and $J(q_5)$ is very small. This agrees with the observation of the 2D diffuse scattering [9], which we also confirmed. In fact, a scan along $(\frac{1}{3}\frac{1}{3}\zeta)$ shows no three-dimensional modulation even at $T_N + 0.5$ K. In addition to the degeneration line, there should exist an interaction which favours the double-Q 120° structure. As shown in figure 5(*e*), the structure is characterized by the $+-+-+-$ rotational directions. One may think that the rotational direction is expressed by $S_i \times S_j$, and hence the Dzyaloshinsky–Moriya interaction may stabilize the structure. However the Dzyaloshinsky–Moriya interaction is prohibited by the space group $R\bar{3}m$ of the α-$NaFeO_2$ structure. We checked small deformation of the structure by x-ray powder diffraction at room temperature, but no superlattice peak was detected.

6. Conclusion

Magnetic ordering in the quasi-two-dimensional antiferromagnet on the stacked triangular lattice $LiCrO_2$ has been studied by means of susceptibility, neutron diffraction and

polarization analysis measurements. The rhombohedral stacking complicates the three-dimensional magnetic configuration. The polarization analysis and the temperature dependence of the magnetic reflection prove that both the c axis and c plane components establish long-range order at a single phase transition temperature T_N. The temperature dependence of the susceptibility strongly suggests that a 120° structure is established in each layer. If the 120° structure in a plane including the c axis is assumed in each layer, neutron data show that magnetic ordering is the double-Q 120° structure with wave numbers $q = (\frac{1}{3}\frac{1}{3}0)$ and $(-\frac{2}{3}\frac{1}{3}\frac{1}{2})$, which is shown in figure 5(*e*). It is characterized by an alternating sequence along the c axis of the rotational direction of the 120° structure. Interactions which stabilize the double-Q 120° structure remain to be clarified.

Acknowledgments

We would like to thank M Nishi and T Inami for assistance in performing the polarization analysis experiment. This work was performed using facilities of the Institute for Solid State Physics, University of Tokyo.

Appendix A.

We will show that the double-Q structure really represents the coplanar $+-+-+-$ 120° structure. We start from the general 6-Q structure (6), and modify it to a more convenient form for the six layers at $z = 0, \frac{1}{3}, \ldots, \frac{5}{3}$. The positional vectors are written as

$$R = \begin{cases} R_0 & z = 0 \\ d + R_0 & z = \frac{1}{3} \\ 2d + R_0 & z = \frac{2}{3} \\ (001) + R_0 & z = 1 \\ d + (001) + R_0 & z = \frac{4}{3} \\ 2d + (001) + R_0 & z = \frac{5}{3} \end{cases} \tag{A1}$$

where $d = (\frac{2}{3}\frac{1}{3}\frac{1}{3})$ and $R_0 =$ (integer, integer, 0). For example, $R_0 = (0, 0, 0)$, $(1, 0, 0)$ and $(2, 0, 0)$ for A_n, B_n and C_n, respectively. Inserting (A1) into (6), we obtain

$$S_R = b_n e^{iq_1 \cdot R_0} + b_n^* e^{-iq_1 \cdot R_0} \qquad z = n/3 \qquad (n = 0, 1, \ldots, 5) \tag{A2}$$

with complex polarization vectors $b_n = b_n' - ib_n''$

$$\begin{aligned} b_0 &= a_1 + a_2 + a_3 + a_4 + a_5 + a_6 \\ b_1 &= \rho a_1 + \rho^* a_2 + a_3 + e^{i\pi/3}(\rho a_4 + \rho^* a_5 + a_6) \\ b_2 &= \rho^* a_1 + \rho a_2 + a_3 + e^{i2\pi/3}(\rho^* a_4 + \rho a_5 + a_6) \\ b_3 &= a_1 + a_2 + a_3 + e^{i\pi}(a_4 + a_5 + a_6) \\ b_4 &= \rho a_1 + \rho^* a_2 + a_3 + e^{i4\pi/3}(\rho a_4 + \rho^* a_5 + a_6) \\ b_5 &= \rho^* a_1 + \rho a_2 + a_3 + e^{i5\pi/3}(\rho^* a_4 + \rho a_5 + a_6) \end{aligned} \tag{A3}$$

where $\rho = e^{i2\pi/3}$. Equation (A2) becomes the $+-+-+-$ 120° structure, if b_n satisfy $b_n = b_0^* \exp(i\beta_n)$, $(n = 1, 3, 5)$, $b_n = b_0 \exp(i\beta_n)$, $(n = 2, 4)$

$$|b_0'| = |b_0''| \qquad b_0' \perp b_0''. \tag{A4}$$

Equations (A3) and (A4) becomes simple if double-Q structures are assumed. If only $|a_1|$ and $|a_5|$ are finite (A3) becomes

$$\begin{aligned} b_0 &= a_1 + a_5 \\ b_1 &= \rho(a_1 - a_5) = \rho b_3 \\ b_2 &= \rho^*(a_1 + a_5) = \rho^* b_0 \\ b_3 &= a_1 - a_5 \\ b_4 &= \rho(a_1 + a_5) = \rho b_0 \\ b_5 &= \rho^*(a_1 - a_5) = \rho^* b_3. \end{aligned} \tag{A5}$$

The double-Q structure becomes the $+-+-+-$ 120° structure, if b_n satisfy

$$b_3 = b_0^* \exp(i\beta) \qquad |b_0'| = |b_0''| \qquad b_0' \perp b_0''. \tag{A6}$$

The resulting structure is shown in figure 5(*e*). The parameter β is the angle between S_{A_0} and S_{A_3}. If the 120° structure is in a plane including the c axis, b_0 is written as

$$b_0 = |b_0'|(e_c - ie_\alpha)\, e^{i\gamma}$$

where e_c and e_α stand for unit vectors along the c axis and in the c plane, respectively, and γ is the angle between S_{A_0} and the c axis. The complex amplitudes a_1 and a_5 are expressed as

$$\begin{aligned} a_1 &= |b_0'|\, e^{i\beta/2}\left[e_c \cos\left(\frac{\beta - 2\gamma}{2}\right) - e_\alpha \sin\left(\frac{\beta - 2\gamma}{2}\right)\right] \\ a_5 &= |b_0'|\, e^{i(\beta-\pi)/2}\left[e_c \sin\left(\frac{\beta - 2\gamma}{2}\right) + e_\alpha \cos\left(\frac{\beta - 2\gamma}{2}\right)\right]. \end{aligned} \tag{A7}$$

From this equation one sees that not β and γ independently but the combination $\beta - 2\gamma$ can be determined by neutron scattering, because the phase factors of (A7) do not affect intensities (3) and (4).

One can reach similar expressions to (A5) for the double-Q structures with (q_2, q_6) and (q_3, q_4). This is a matter of course, because they can be derived by the threefold symmetry around the c axis. The other double-Q structures such as that with (q_1, q_4) can easily be shown not to express the $+-+-+-$ 120° structure. Therefore we conclude that only three double-Q structures with (q_1, q_5), (q_2, q_6) and (q_3, q_4) can be the $+-+-+-$ 120° structure.

References

[1] Wannier G H 1950 *Phys. Rev.* **79** 357
Stephenson J 1964 *J. Math. Phys.* **5** 1009

[2] Miyashita S and Shiba H 1984 *J. Phys. Soc. Japan* **53** 1145

[3] Kawamura H and Miyashita S 1984 *J. Phys. Soc. Japan* **53** 9
Kawamura H and Miyashita S 1984 *J. Phys. Soc. Japan* **53** 4138

[4] Anderson P W 1973 *Mater. Res. Bull.* **8** 153
Fazekas P and Anderson P W 1974 *Phil. Mag.* **30** 423

[5] Rastelli E and Tassi A 1986 *J. Phys. C: Solid State Phys.* **19** L423; 1987 *J. Phys. C: Solid State Phys.* **20** L303; 1988 *J. Phys. C: Solid State Phys.* **21** 1003; 1988 *J. Appl. Phys.* **63** 3823; 1989 *Physica* B **156 & 157** 115

[6] Jansen A P J 1986 *Phys. Rev.* B **33** 6352
Reimers J N and Dahn J R 1992 *J. Phys.: Condens. Matter* **4** 8105

[7] Delmas C, Le Flem G, Fouassier C and Hagenmuller P 1978 *J. Phys. Chem. Solids* **39** 55
Delmas C, Menil F, Le Flem G, Fouassier C and Hagenmuller P 1978 *J. Phys. Chem. Solids* **39** 51

[8] Soubeyroux J L, Fruchart D, Delmas C and Le Flem G 1979 *J. Magn. Magn. Mater.* **14** 159
[9] Soubeyroux J L, Fruchart D, Marmeggi J C, Fitzgerald W J, Delmas C and Le Flem G 1981 *Phys. Status Solidi* **67** 633
[10] Suzuki M, Yamada I, Kadowaki H and Takei H 1993 *J. Phys.: Condens. Matter* **5** 4225
[11] Ajiro Y, Kikuchi H, Sugiyama S, Nakashima T, Shamoto S, Nakayama N, Kiyama M, Yamamoto N and Oka Y 1989 *J. Phys. Soc. Japan* **57** 2268
[12] Doumerc J-P, Wichainchai A, Ammar A, Pouchard M and Hagenmuller P 1986 *Mater. Res. Bull.* **21** 745
[13] Kadowaki H, Kikuchi H and Ajiro Y 1990 *J. Phys.: Condens. Matter* **2** 4485
[14] Oohara Y, Mitsuda S, Yoshizawa H, Yaguchi N, Kuriyama H, Asano T and Mekata M 1994 *J. Phys. Soc. Japan* **63** 847
[15] Hirakawa K, Ikeda H, Kadowaki H and Ubukoshi K 1983 *J. Phys. Soc. Japan* **52** 2882
[16] Watson R E and Freeman A J 1961 *Acta Crystallogr.* **14** 27
[17] Kadowaki H, Ubukoshi K, Hirakawa K, Martinez J L and Shirane G 1987 *J. Phys. Soc. Japan* **56** 4027
[18] Kadowaki H, Ubukoshi K and Hirakawa K 1987 *J. Phys. Soc. Japan* **56** 751
[19] Oohara Y, Kadowaki H and Iio K 1991 *J. Phys. Soc. Japan* **60** 393